Application of the Characteristic Basis Function Method for the Electromagnetic Analysis of Electrically Large and Complex Bodies

Carlos Delgado [1], Eliseo García [2], Felipe Cátedra [1], and Raj Mittra [3]
[1] Department of Computer Science
University of Alcalá, Edificio Politécnico, Alcalá de Henares 28871, SPAIN
carlos.delgado@uah.es , felipe.catedra@uah.es

[2] Department of Automatics
University of Alcalá, Edificio Politécnico, Alcalá de Henares 28871, SPAIN
eliseo.garcia@uah.es

[3] Department of Electrical Engineering
Pennsylvania State University, University Park, PA 16802, USA
Mittra@engr.psu.edu

***Abstract*—** An overview of a parallel implementation of the Characteristic Basis Function Method combined with the Multilevel Fast Multipole Algorithm is presented. This approach allows an accurate analysis of very large electromagnetic problems. The geometry is described by means of Non-Uniform Rational B-Splines, and the macro-basis functions are expressed in terms of subsectional functions totally conformed to the original geometry. A number of representative examples are considered in order to show the performance of the proposed approach.

***Index Terms*—** Method of Moments, Macro-Basis Functions, Characteristic Basis Function Method (CBFM).

I. INTRODUCTION

Due to the great improvement of the computational efficiency during the last decade, many problems for which high-frequency approaches (such as Physical Optics [1] or the Geometrical Theory of Diffraction [2]) or hybrid methods [3-6] were the only possible choices are now amenable to simulation via rigorous techniques. Also, the development of architectures and paradigms for the parallelization of computer codes [7] are playing a very important role in the expansion of the scope of rigorous analysis methods. However, the most important contribution to this new scenario is given by the development of improved numerical techniques carried out by numerous research groups worldwide. Even though the heterogeneous underlying strategies define different features for each of these developments, we can classify them into different categories, according to the treatment of the electromagnetic problem.

The Method of Moments (MoM) [8] is nowadays a strong reference against which the new frequency-domain approaches can be compared. Since in the MoM the unknowns are distributed over the surface of the objects, it is widely used for the analysis of scattering or radiation problems involving geometries with one or several layers of homogeneous materials. Many of the new approaches maintain a MoM-based formulation and add new improvements that allow us to expand its application range. The main drawback of the MoM is the size of the coupling matrix that determines the linear system to be solved later. Owing to a fine discretization of the object geometry, typically 10 per λ in the conventional MoM, the matrix size becomes large relatively quickly as the object size becomes electrically large, and this, in turn, places a heavy burden on the CPU, both in terms of solve time and memory. A widely well-known approach to overcome this difficulty consists of using the Fast

Multipole Method (FMM) [9] or the Multilevel Fast Multipole Algorithm (MLFMA) [10], that reduce the computational complexity from $O(N^2)$ to $O(N^{3/2})$, or even to $O(N\log N)$ for the latter approach. The use of these approaches entails the storage of only the near-field terms of the coupling matrix and computing the far-field interactions efficiently via fast matrix-vector products in the iterative solution process. There are a number of techniques that also take advantage of the efficient evaluation of these products in the iterative solution of large problems, such as the Complex Multipole Beam Approach (CMBA) [11], the Impedance Matrix localization (IML) technique [12] or the Adaptive Integral Method (AIM) [13].

A different strategy which has been proven to decrease the computational complexity of the conventional MoM is based on the fact that the submatrices that contain the coupling between moderately distant blocks (about a few wavelengths, usually) are rank-deficient or, in other words, the number of degrees of freedom is smaller than the number of samples used. Therefore, these submatrices can be compressed using some of the techniques available in the literature, like those based on the Modified Gram-Schmidt procedure (MGS) [14, 15], the Adaptive Cross Approximation (ACA) [16, 17] or the Matrix Decomposition Algorithm [18]. It is worthwhile to remark that these approaches make use of purely algebraic manipulations of the original matrices.

A third group of methods, among which the presented work can be situated, is based on a strategy that utilizes a domain-decomposition scheme and reduces the number of unknowns by replacing the subdomain-type basis functions with a set of macro-basis functions. We can mention here the Synthetic Function Expansion technique (SFX) [19] or the Characteristic Basis Function Method (CBFM) [20].

The CBFM models the current on an arbitrarily shaped target by means of a set of macro-basis functions, called Characteristic Basis Functions (CBFs), defined over geometrical blocks in which the geometry is subdivided. Instead of being limited to a predetermined and/or fixed shape, the CBFs are generated taking into account the physics of the problem, so they are tailored to the geometrical properties of each block, and their use leads to a "reduced" matrix whose size is considerably smaller than that of the original impedance matrix based on subdomain functions (e.g. Rao-Wilton-Glisson functions [21] or rooftops [22]). Each CBF, in turn, can be seen as an aggregation of low-level basis functions whose weights are fixed when each CBF is generated. The reduction in matrix size achieved by the CBFM enables us to use direct solvers for some problems where, previously, an iterative solver represented the only possible choice because of the size of the impedance matrix. However, for very large problems the reduction achieved in the number of unknowns may still be insufficient as to resort to a direct solver. In this situation, an iterative solution process can be utilized by combining the CBFM with the MLFMA approach [23].

We will consider in this work a geometric representation based on Non-Uniform Rational B-Splines (NURBS) [24], due to its flexibility to model arbitrary geometries and the fact that this format has become widespread in the world of Computer Aided Geometric Design (CAGD). The CBFs are represented in terms of modified rooftop functions defined along the u or v directions over a parametric domain, totally conformed to the NURBS patches, so the discretization error is minimized.

This paper is structured as follows. In Section 2, we discuss the procedure for obtaining the Characteristic Basis Functions from rigorous or asymptotic solutions of smaller problems where each block is isolated from the rest of the geometry. Section 3 deals with a particular implementation of the CBFM, used in this work, where the low-level basis functions employed are modified rooftops placed over the parametric domain of NURBS patched and totally conformed to the surface, and the low-level testing functions are razor blades also located directly over the parametric domain of the patch. In Section 4 the applicability of the CBFM is enlarged by including the MLFMA formulation, so that the computational requirements of very large problems are now affordable by using the CBFM-MLFMA. In section 5 we discuss the details of the parallelization of the proposed approach in order to optimize the balance of the computational load between different computing nodes. Finally we present some conclusions derived from this work.

II. GENERATION OF THE CHARACTERISTIC BASIS FUNCTIONS

Previous to the generation of the CBFs, which will model the current over the structures under analysis, we set up a partitioning of the geometry into blocks. It is important to note that the size of these blocks can go up to a few thousands low-level basis functions. The CBF generation process takes into account the shape of each block. In order to incorporate the physics of the problem into the CBFs we obtain these functions from the current solutions of the isolated block. The approach shown in [20] considers a scheme where the CBFs are grouped into two categories: the primary CBFs, due to the currents induced by the incident field on each block (obtained by isolating the block), and the secondary CBFs, obtained by assuming that the incident field on a block is due to the field radiated by the currents that the external field induces on another block. Thus, a set of CBFs (one primary and several secondary CBFs) is assigned to each block. However, by following this approach the reduced matrix depends on the external field, which can be undesirable in some cases. In order to overcome this problem, there is a different technique, more appropriate for scattering problems with multiple right hand sides, consisting on obtaining the CBFs from a set of plane waves (Plane Wave Spectrum, PWS) which impinge on the scatterer from different angles, and considering both polarizations (θ and φ). By following this procedure we eliminate the primary and secondary classification of the CBFs. Fig. 1 depicts this approach in a 2D scenario. The different plane waves that surround the surface are separated by an angular step $\Delta\theta$. The number of plane waves to be considered obviously depends on the size of the block. In fact, having a large enough number of currents with different shapes based on approximate solutions with which build the new basis functions (i.e., the CBFs) is more important than having a few extremely accurate solutions of the currents due to several plane waves. It is also interesting to remark that the accuracy obtained in the modelization of evanescent fields can be controlled by increasing the discretization density (i.e. the size of the subdomains). The evanescent behaviour of the CBFs is seen after obtaining the currents induced by the plane waves on the block with the MoM. Therefore, it is not necessary to consider a sampling of plane waves outside of the visible spectrum in order to obtain CBFs with fast amplitude variations. Thus, simply by choosing an angular separation in the θ and φ spherical components between consecutive plane waves depending on the block size is enough for obtaining good results. Specifically, we use a separation of 10º for block sizes whose maximum side length is below 2λ, 5º when the block size is up to 4λ and 3º for larger blocks.

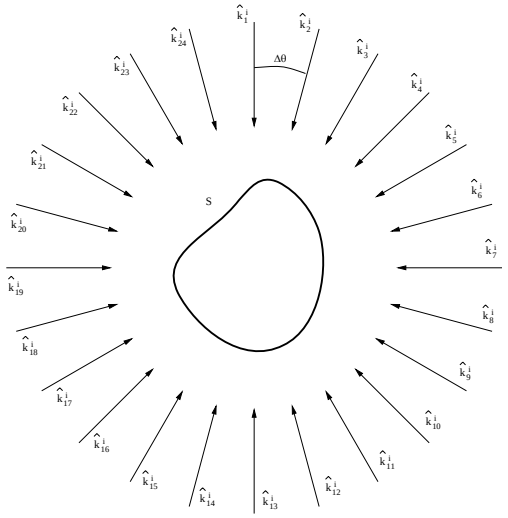

Fig. 1. 2D scheme of the PWS surrounding the target object for the CBF generation.

There are different possibilities for obtaining the currents induced by the plane waves on the block under consideration. For example, the conventional Method of Moments can be used for this purpose. If we are considering P different incident waves, it would be necessary to solve the following set of MoM problems [20,25]:

$$[Z]^i [J]_k^i = [V]_k^{inc}, \; k = 1,...,P, \qquad (1)$$

where $[Z]^i$ is the coupling matrix for block-*i*, $[J]_k^i$ indicates the current vector for block-*i* and the k^{th} plane wave excitation, and $[V]_k^{inc}$ represents the k^{th} excitation vector. Due to the fact that we are isolating the block from the rest of the geometry, in order to mitigate the artificial edge behaviour of the currents it is convenient to compute the currents over an extension of the original block, usually considering a fraction of wavelength as the size of this extension [20]. Only the currents that

are inside the original block are retained and stored as the CBFs after being orthogonalized. Obviously, we do not need to follow this procedure if we are using PO to calculate the induced currents instead of the MoM. The size of the extension depends on the type of low-level basis functions considered. We have found that with the scheme described in [28], which utilizes rooftops, no extension is required to get accurate results, because of the use of connection strips which effectively dovetail the subdomains in which the low-level basis functions are defined. For an RWG-based scheme, accurate results are obtained by extending the original blocks by approximately 0.3λ. If no extensions are considered, a noticeable degradation of the results has been observed in a number of test cases simulated.

It is also possible to use high-frequency approaches for the computation of the currents induced by the incident plane wave, when the block being analyzed is smooth. The PO approach can be used to bypass the solution of (1) for different plane wave excitations. The expansion of the current over the block-*i* in terms of subdomain functions due to the k-th incident plane wave can be expressed as:

$$B_k^i(u,v) = 2\sqrt{\frac{\mu_0}{\varepsilon_0}}\sum_{n=1}^{N_i}\left\{\hat{n}(u_{0n},v_{0n})\times\left[\hat{k}_k^i\times\vec{E}_0\right]\cdot \exp\left[-jK\left(\hat{k}_k^i\cdot\vec{r}(u_{0n},v_{0n})\right)\right]\cdot T_n(u,v),\right. \quad (2)$$

where (u_{0n}, v_{0n}) designates the point on the nth rooftop where the current is sampled, and corresponds to the center of the associated parametric contour, $\hat{n}$ is the normal vector and $\vec{r}$ is the spatial point. The function $T_n(u,v)$ is the nth rooftop located in block-*i*, and N_i is the total number of rooftops within this block. Our experience shows that PO currents can be used to construct the Characteristic Basis Functions even for relatively small block sizes (one wavelength or even less). One can find that in some cases the PO-derived CBFs cannot model appropriately the fast current variations in the free edges of the geometry. The scheme shown in [26] solves this problem by defining a special type of blocks with a reduced width near these edges.

After generating the induced current vectors corresponding to each one of the plane wave excitations for block-*i*, the associated CBFs can be obtained by performing the orthogonalization of these vectors. The Singular Value Decomposition (SVD) [14] is used for this purpose. If we denote as *M* the total number of plane waves considered, we can arrange all the calculated currents in a $M \times N$ matrix form, where *N* is the number of low-level basis functions on the block. After calculating the SVD of this matrix, we obtain a new orthogonal set of basis vectors which can be identified with the singular vectors resulting from the SVD operation [27]. However, it is not necessary to retain the complete set of singular vectors as the new macro-basis functions. Those singular vectors which correspond to singular values with a negligible magnitude can be discarded without losing accuracy in the final results. In other words, we set a threshold γ, relative to the largest singular value, and retain only the singular vectors corresponding to those singular values above γ times the strongest singular value. We recommend γ in the range from $2\cdot10^{-3}$ to10^{-3}. It is important to remark that the number of orthogonal vector retained after the SVD is usually several times lesser than the number of original plane wave currents, due to the linear relations of dependence of these in the block surface. The induced current solutions used to represent the CBFs need only be approximate solutions at this stage, since the final solution will be derived later by adjusting the coefficients of these basis functions. In other words, as long as we introduce a sufficiently large number of plane waves for the CBF generation, the final current distribution will be satisfactorily modelled. The truncated SVD technique referenced in the manuscript is not an exact decomposition of the original matrix, but it is a very useful and close approximation to the original matrix achieved by a matrix of reduced rank (optimal approximation considering the Frobenius norm). In the practical applications we observe a very rough decrease of the amplitude of the singular values. In most cases setting the threshold higher that the reference value given in the manuscript does not affect significatively the number of resulting CBFs. The threshold values proposed in this work allow us to obtain very good results (in the sense that the

resulting set of CBFs can model the currents very accurately) and do not depend on the shape or the size of the block.

In Fig. 2 we have depicted the evolution of the magnitude of the singular values for two different block types and sizes. We show in the figure the singular values obtained for a plane block with a side length of two wavelengths and for a block with the shape of a spherical quadrant with a radius of one wavelength. It can be seen that the magnitude of these values decays very fast. The contribution of those CBFs whose singular values have a very small magnitude can be considered negligible, so that they can be discarded.

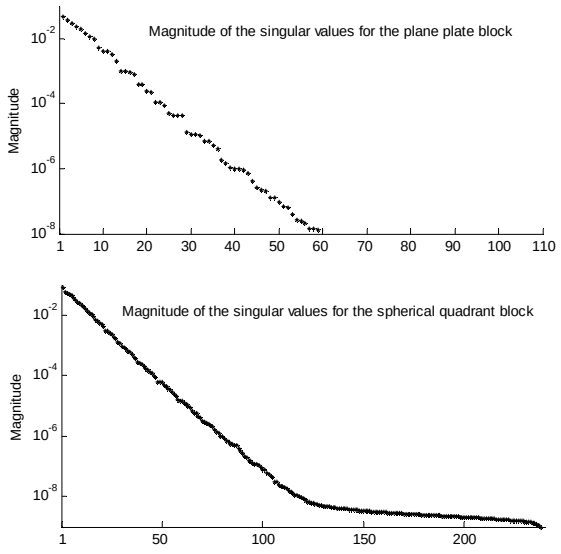

Fig. 2. Magnitude of the singular values after calculating the currents induced by the plane waves on the block for a plane plate case (top) and a spherical quadrant case (bottom).

III. THE COMBINATION OF THE CBFM AND NURBS SURFACES

As previously indicated, the CBFM is independent from the type of low-level subsectional basis functions chosen for the expansion of the CBFs. In this work, we consider a generalization of the planar rooftops introduced by Glisson and Wilton in [22] as the low-level basis functions. These functions are located over a region of the NURBS patch where they belong. To do this, the parametric domain associated to the NURBS surface is divided in order to generate a mesh of rectangular subdomains. Each one of the contour segments between two consecutive subdomains is then associated with a basis and a testing function. It is necessary to define two sets of rooftops, for modeling the *u*- and *v*-components of the current over the patch. The testing functions selected are razor-blades, also be separated into two groups. For the Electric Field Integral Equation (EFIE) formulation we place the razor blades perpendicular to the contour shared by each pair of subdomains, while they should be parallel to the contour for the case of the Magnetic Field Integral Equation (MFIE). Note that these basis and testing functions are totally conformed to the NURBS surface. Figure 3 shows a scheme of an arbitrary surface with its control points, and the set of subdomains obtained when we divide its parametric domain into regions. Also, we show in the figure how a basis function along the *v*-direction and a testing function along the *u*-direction are placed. Note that this testing function corresponds to the EFIE formulation, according to the above explanation (perpendicular to the contour shared between two subdomains). Further details can be consulted in [28-30].

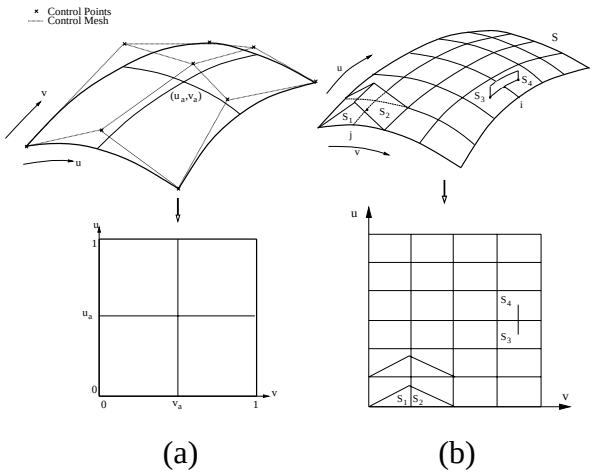

Fig. 3. (a): Arbitrary NURBS patch and control points; (b): Discretization of the surface in the parametric domain and collocation of basis and testing functions.

As a validation of the CBFM approach described so far in this work, we consider a PEC cube with two square facets parallel to each canonical plane (*XY*, *XZ* and *YZ*). The length of each side is 1 meter, and a frequency of 900 MHz has been set for the simulations. We have obtained monostatic RCS values and we have compared

them with those returned by the conventional MoM, for the θ-θ and φ-φ polarizations. Figures 4 and 5 show a good agreement between the results obtained using both methods. The number of unknowns required by the Method of Moments has been 11532, while the CBFM has needed 1140 unknowns. Each one of the six faces of the cube was identified as one CBFM block, so we obtained 190 CBFs for each block. The CBFs have been obtained from a set of incident plane waves considering $\Delta\theta=\Delta\varphi=7^{o}$. The MoM CPU time is 44022 seconds; the CBFM CPU-time is 3526 seconds. Both results have been obtained using a SUN Fire V65 workstation (2 Xeon 3GHz processors with 8 Gbytes of RAM).

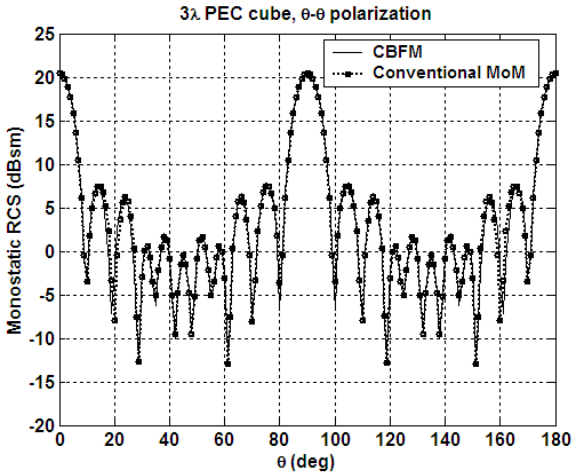

Fig. 4. θ-θ polarization results for the PEC cube monostatic RCS analysis.

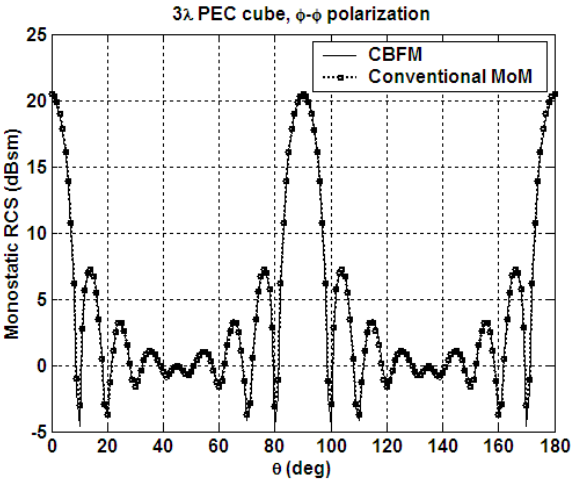

Fig. 5. φ-φ polarization results for the PEC cube monostatic RCS analysis.

In the following test case we consider the COBRA cavity with a flap (Fig. 6), modeled using 24 NURBS surfaces. In figures 7 and 8 we show the monostatic RCS results obtained for an angular sweep with a fixed value of $\varphi=0^{o}$ and $\theta=0^{o}$ to 90^{o} with an angular step of 1^{o} at a frequency of 10 GHz with the proposed method, compared with the values given by the Finite Element-Boundary Integral method in [31]. From the discretization process, 59147 unknowns arise considering the standard sampling rate of $\lambda/10$. An angular step of 5^{o} has been considered in this case for the CBF computation. Only 4711 high-level functions have been retained after orthogonalizing the PO-derived induced currents. The simulation has been carried out in 65966 seconds using an Opteron processor at 2.4 GHz with a total RAM of 64 Gbytes

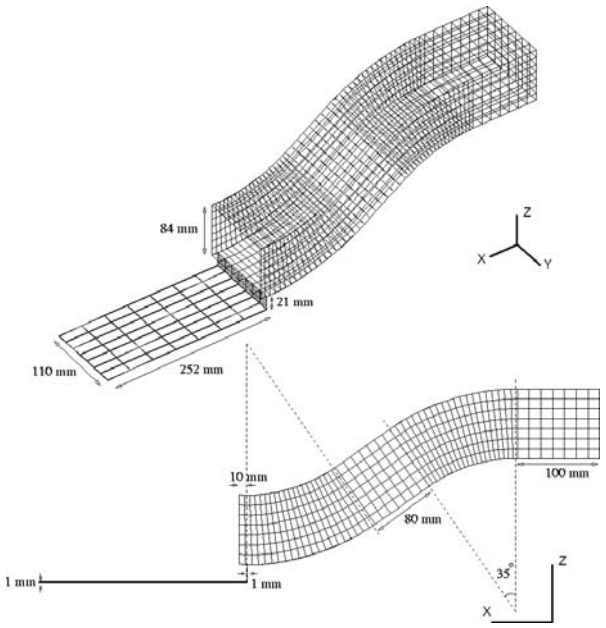

Fig. 6. Geometrical scheme of the COBRA cavity with a flap.

The next example consists of a PEC almond-shaped target (Fig. 9), similar to the NASA almond [32], but with a different size. The total length of the object is 2.5 meters with a total surface area of 4 m^2. The geometry is defined by the equations:

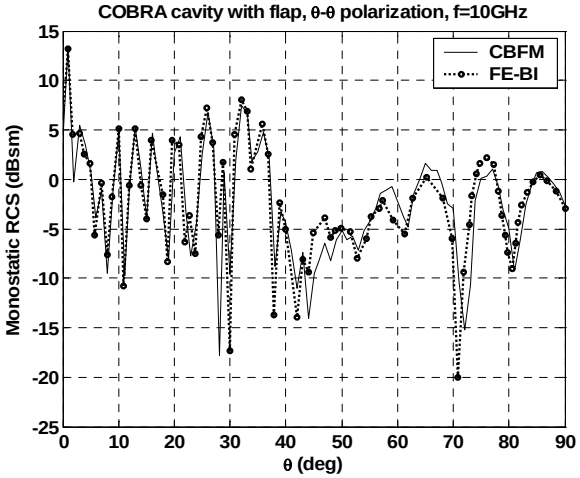

Fig. 7. θ-θ polarization results for the COBRA cavity with a flap.

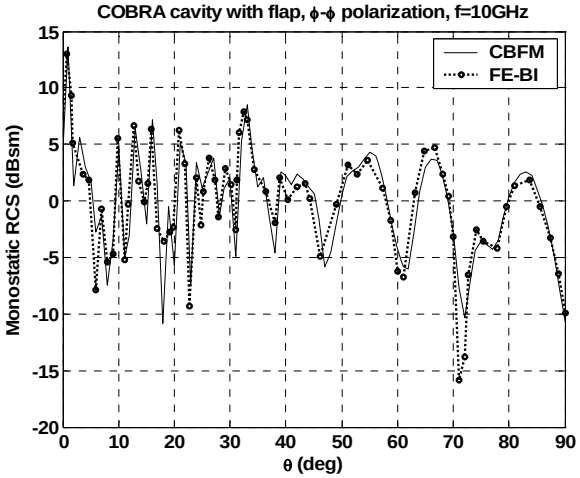

Fig. 8. φ-φ polarization results for the COBRA cavity with a flap.

$$\begin{aligned} x &= dt \\ y &= 0.193333\, d\left[\sqrt{1-\left(\frac{t}{0.416667}\right)^2}\right]\cos\psi \\ z &= 0.06444\, d\left[\sqrt{1-\left(\frac{t}{0.416667}\right)^2}\right]\sin\psi \\ -\pi &< \psi < \pi \end{aligned} \quad \text{, for } -0.416667 < t < 0 \tag{3}$$

$$\begin{aligned} x &= dt \\ y &= 4.833450\, d\left[\sqrt{1-\left(\frac{t}{2.083350}\right)^2}-0.96\right]\cos\psi \\ z &= 1.611148 d\left[\sqrt{1-\left(\frac{t}{2.083350}\right)^2}-0.96\right]\sin\psi \\ -\pi &< \psi < \pi \end{aligned} \quad \text{, for } 0 < t < 0.583333 \tag{4}$$

where d is the length of the almond, 2.5 m.

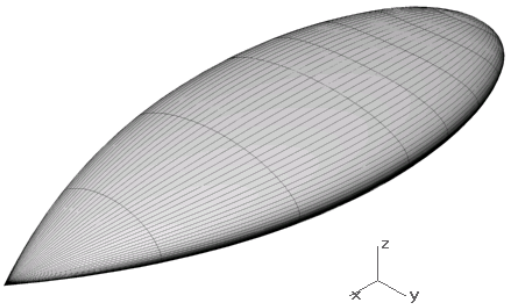

Fig. 9. "Almond" test case.

Figures 10 and 11 show the bistatic RCS results at a frequency of 2 GHz for the θ-θ and φ-φ polarizations, respectively. We have compared the MoM results with those obtained by utilizing the CBFM with PO-derived CBFs. We have considered 181 observation directions ranging from φ=0º to φ=180º, for an incidence angle given by θ =90º and φ=180º. The number of unknowns is 55460 when using the MoM, while 5801 CBFs are retained in the CBFM approach. The almond is modeled using 8 NURBS patches which, in turn, are identified as 8 CBFM blocks, so the average number of CBFs and low-level unknowns per block are 725 and 6932, respectively. Both cases show good agreement. The total time needed to solve this case example has been 12123 seconds using the same machine as in the previous cases.

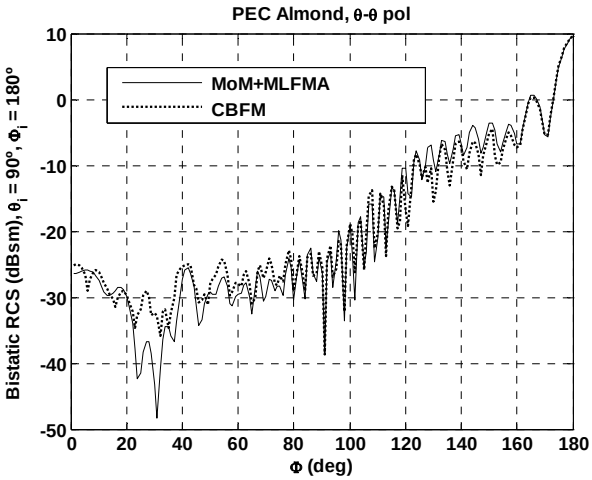

Fig. 10. Bistatic RCS results for the almond test case, θ-θ polarization.

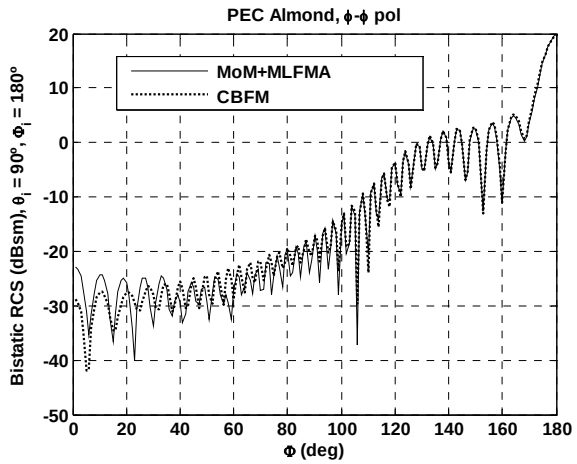

Fig. 11. Bistatic RCS results for the almond test case, φ-φ polarization.

IV. COMBINATION OF MLFMA AND CBFM

In previous sections, we showed the advantages of CBFM in terms of the reduction of the number of unknowns, leading to a coupling matrix whose size is much smaller than that obtained in the conventional Method of Moments. As a consequence, direct solvers can be applied to solve medium size problems, which could be addressed in the past by relying upon iterative techniques.

However, when the size of the scatterer becomes very large, the CBFM system matrix can become so large as to preclude its solution without resorting to iteration, despite a significant reduction in the matrix size realized via the CBFM. Additionally, the memory needed to store the reduced matrix can present a problem as well. One of the most common approaches to easing the burden on the computational resources entails the storing of only the near-field terms of the coupling matrix and computing the far-field interactions via the Fast Multipole Method, or its multilevel implementation, MLFMA. The use of the MLFMA avoids the need of calculate and store the coupling terms between near elements in the reduced matrix, thereby optimizing the memory storage requirements. In addition, the MLFMA improves the CPU-time required to solve the system via an efficient evaluation of the matrix-vector product operations in an iterative solution process. In the application of the MLFMA we compartmentalize the whole geometry into several first-level cubical groups which, in turn, generate higher-order cubes as they are grouped. A first-order group size of a quarter of wavelength is recommended [10], and the aggregation point of every cube is chosen to be its geometrical centre. For the first level, the cubes include a few basis functions, and the coupling between basis functions associated to geometrically close cubes is calculated in a rigorous way and stored for later use. Figure 12 depicts the volumetric distribution of these cubical volumes, given a generic geometry.

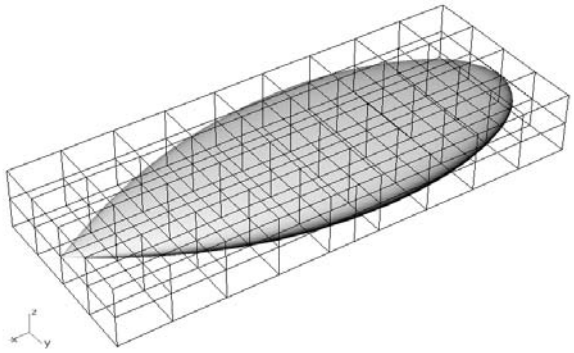

Fig. 12. Compartmentalization of the target geometry into cubical groups.

The application of the FMM/MLFMA entails the storage of only the near-field terms of the coupling matrix and the efficient computation of the far-field interactions in the iterative process. This is achieved by computing the matrix-vector products as shown in (5). For both the EFIE and MFIE cases we have:

$$A_{ji} = \int V_{mj}^{\begin{Bmatrix} AGG-EFIE \\ AGG-MFIE \end{Bmatrix}}(\hat{k})\tau_{mm'}(\hat{k},\vec{r}_{mm'})V_{m'i}^{\begin{Bmatrix} DIS-EFIE \\ DIS-MFIE \end{Bmatrix}}(\hat{k})d^2\hat{k} \quad , \quad (5)$$

where $V_{mj}^{AGG}(\hat{k})$ represents the aggregation term, computed as follows for each formulation:

$$\begin{aligned} V_{mj}^{AGG-EFIE}(\hat{k}) &= \sum_{k=1}^{N_m}\int_u\int_v e^{-j\hat{k}\cdot\overrightarrow{r_{jm}}}(\bar{I}-\hat{k}\hat{k})T_k(u,v)dudv \\ V_{mj}^{AGG-MFIE}(\hat{k}) &= -\hat{k}\times\sum_{k=1}^{N_m}\int_u\int_v e^{-j\hat{k}\cdot\overrightarrow{r_{jm}}}\left[T_k(u,v)\times\hat{n}(u,v)\right]dudv \end{aligned} \quad , \quad (6)$$

where N_m is the number of subdomain functions within the cubical group, and $\vec{r}_{j,m}$ represents the vector that extends from the sampling point to the aggregation point. Analogously, the dissagregation term can be computed as:

$$V_{m'i}^{DIS-EFIE}(\hat{k}) = \sum_{k=1}^{N_m} \int_u \int_v e^{j\hat{k}\cdot\overline{r_{im'}}} (\bar{I} - \hat{k}\hat{k}) R_k(u,v) du dv \quad , \quad (7)$$
$$V_{m'i}^{DIS-MFIE}(\hat{k}) = \sum_{k=1}^{N_m} \int_u \int_v e^{j\hat{k}\cdot\overline{r_{im'}}} R_k(u,v) du dv$$

and the translation term between points *m* and *m'* is given by:

$$\tau_{mm'}(\hat{k}, \vec{r}_{mm'}) = \frac{jk}{4\pi} \sum_{l=0}^{L} j^l (2l+1) h_l^{(1)}(kr_{mm'}) P_l(\hat{r}_{mm'} \cdot \hat{k}), \quad (8)$$

where $h_l^{(1)}(x)$ is a spherical Hankel function of the first kind and $P_l(x)$ is a Legendre polynomial.

The first step in the computation of the far-field interactions embodies calculating the aggregation terms for each first-level cube, according to (6). These terms represent the outgoing wave expansions of each cube. For each higher-level cube, the aggregation is obtained by taking into account the aggregation terms of the lower-level cubes contained in it, and by using shifting and interpolation in order to reduce the computational resources. After the aggregation stage, translation between well-separated cubes that belong to the same level is performed.

The last step of the algorithm consists of the disaggregation process, in which all the cubes have received the contributions from the rest of the cubes belonging to the same level, and these contributions are released to their children cubes, via shifting and anterpolation. If the parent cube is a first-level cube, the contribution released to the subdomain functions is given by (7).

Following the MLFMA strategy, the scatter geometry is compartmented into several first-level groups and higher-order cubes are generated. Each high-level cube groups several cubes in the lower level and so on. According to this idea, a tree structure is created from the highest level to the first one.

Next, the CBFM blocks are defined and the macro-basis functions are obtained via SVD as it was shown in previous sections. Each CBF included in a block extends over the entire block, so its size is usually much larger than the size of the subdomains. Therefore, it is common that a CBF can be defined over several MLFMA groups.

It shall be pointed out that the size of the groups and the corresponding number of levels in the application of the MLFMA can be different when we are dealing with CBFs instead of low-level basis functions. In the conventional MoM-MLFMA application, it is recommended to maintain a size of about 0.25 λ for the first level groups. However, in the presented scheme (CBFM-MLFMA) the size of the groups of the first level should be as small as possible, but with the restriction that it is not much smaller than the size of the blocks (the surfaces over which the CBFs extend). From our experience, the best choice for the size of the groups at the first level is between the half and the whole size of the CBF block. If a block extends over many small groups we would require a large amount of memory usage, since each group included in a block must store the multipole information for all the CBFs in that block.

The reduced matrix is calculated containing only the coupling terms between near blocks, which are on or close to the diagonal of the matrix. The reaction terms corresponding to distant are efficiently calculated using the MLFMA. Considering the EFIE formulation, we compute the aggregation for the CBF j inside the block m as follows:

$$V_{mj}^{AGG-EFIE}(\hat{k}) = \sum_{n=1}^{N_n} \alpha_{j,n} V_{m,n}^{AGG-EFIE} = \sum_{n=1}^{N_n} \alpha_{j,n} \int_u \int_v e^{-j\hat{k}\cdot\overline{r_{jm}}} (\bar{I} - \hat{k}\hat{k}) T_n(u,v) du dv \quad , \quad (9)$$

where $\alpha_{j,n}$ is the coefficient of the CBF-*j* associated to the n^{th} basis function T_n, and $V_{m,n}^{AGG-EFIE}$ is the aggregation term for the n^{th} basis function inside the block *m*. Analogously, the dissagregation term can be computed as:

$$V_{m'i}^{DIS-EFIE}(\hat{k}) = \sum_{n=1}^{N_n} \alpha_{j,n} V_{m,n}^{DIS-EFIE} = \sum_{n=1}^{N_n} \alpha_{i,n} \int_u \int_v e^{j\hat{k}\cdot\overline{r_{im'}}} (\bar{I} - \hat{k}\hat{k}) R_n(u,v) du dv \quad , \quad (10)$$

and the translation term between points *m* and *m'* is calculated according to (8).

For the MFIE formulation, the aggregation and disaggregation terms for the CBFs are computed as:

$$V_{mj}^{AGG-MFIE}(\hat{k}) = \sum_{n=1}^{N_n} \alpha_{j,n} V_{m,n}^{AGG-MFIE} = \sum_{n=1}^{N_n} \alpha_{j,n} \int_u \int_v e^{-j\hat{k}\cdot\overrightarrow{r_{jm}}} T_n(u,v)\,du\,dv \quad , \qquad (11)$$

$$V_{m'i}^{DIS-MFIE}(\hat{k}) = \sum_{n=1}^{N_n} \alpha_{j,n} V_{m,n}^{DIS-MFIE} = \sum_{n=1}^{N_n} \alpha_{i,n} (-\hat{k} \times \int_u \int_v e^{j\hat{k}\cdot\overrightarrow{r_{im'}}} R_n(u,v) \times \hat{n}\,du\,dv) \quad . \qquad (12)$$

The previous expressions can be used for solving the problem employing an iterative algorithm. The coupling terms corresponding to geometrically close blocks can be calculated by means of direct matrix-vector products, while far-field coupling terms can be computed through the MLFMA. As a consequence, the CPU-time is reduced, while simultaneously optimizing the memory storage requirements, since the number of CBFs is much smaller than the number of subdomains. It is important to note that the aggregation and disaggregation terms are computed for the CBFs, which allows the analysis of electrically larger problems. Obviously, the CBF generation process increases the preprocessing CPU-time, as will be seen in the numerical examples shown below. However, as the electrical size of the problem increases the preprocessing time is smaller compared to the CPU-time required for the system solution, which in turn involves a higher efficiency of the presented approach when compared to the MoM-MLFMA technique.

It is also interesting to make a remark about the appropriate group and block size in the CBFM-MLFMA combination. The reduction in the number of unknowns depends only on the block size, as the memory requirements depends on the group and block size. From the experience obtained in this work and previous ones, we conclude that block sizes from λ to 2λ and group sizes from 0.5λ to λ constitute a good compromise.

The first test case considered for the validation of the CBFM-MLFMA approach is the COBRA cavity with a cap previously depicted in Fig. 6. We have obtained monostatic RCS values at a frequency of 10 GHz for an angular sweep θ from 0º to 90º with a fixed value of φ=0º. Results for both the θ–θ and φ–φ polarizations are showed in Figures 13 and 14, respectively, in which we compare the MoM-MLFMA technique, the conventional CBFM and the CBFM-MLFMA approach. The conventional MoM-MLFMA approach required about 304000s for the θ-θ polarization and 456000s for the φ-φ polarization using the EFIE formulation and the BiCGStab solver without any preconditioner. As indicated in a previous section, the conventional CBFM CPU-time was 65966 seconds for each polarization. The presented CBFM-MLFMA approach required 23821s for the θ-θ polarization and 27544s for the φ-φ polarization with the same solver used for the MoM-MLFMA case. All the simulations have been performed using an Opteron processor at 2.4 GHz with a total RAM of 64 Gbytes.

The next case consists of two parallel square plates with a size of 32λ and a separation of 16λ between them. The frequency considered is 2.4 GHz. Bistatic RCS values for an incidence direction defined by θ=0º and φ=0º and a sweeping θ from 0º to 180º for the θ-θ polarization have been obtained. Figure 15 shows the results obtained compared with the MoM -MLFMA, and Table 1 contains the corresponding CPU-times and the resulting number of unknowns considered. Regarding the memory comparision between MoM-MLFMA and CBFM-MLFMA, the former approach needs 9.9 Gbytes of RAM while the latter only requires 6.7 Gbytes, for a group size of λ.

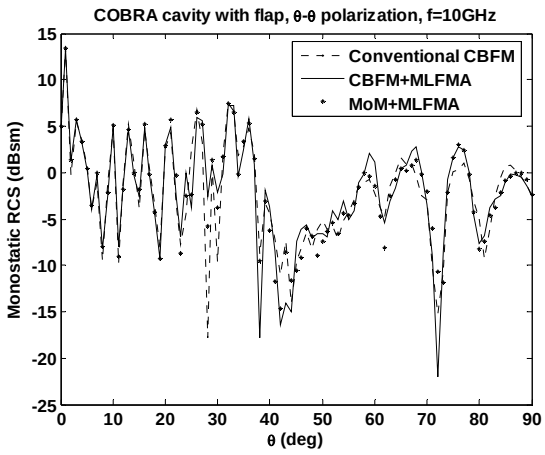

Fig. 13. θ-θ polarization results for the COBRA cavity with a flap.

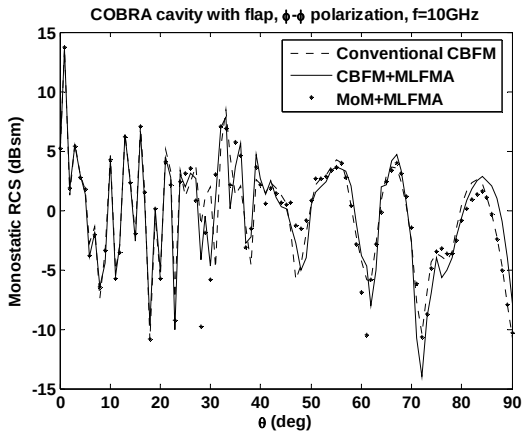

Fig. 14. φ-φ polarization results for the COBRA cavity with a flap.

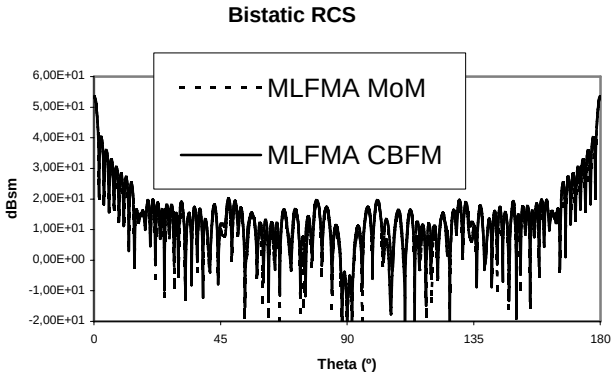

Fig. 15. Bistatic RCS values at 2.4 GHz for the two-plate test case.

Table 1: Analysis of the RCS of the two-plate test case at 2.4 GHz

Method	Block size	Group size	N. Unknowns	Pre-process time (seconds)	Time per direction (seconds)
MoM		0.25	405320	14715	30240
CBFM	1	0.5	105856	22394	5432
CBFM	2	0.5	56832	47357	5213
CBFM	1	1	56832	50695	3105

V. PARALLELIZATION OF THE MLFMA-CBFM APPROACH

It is also important to recognize that currently the parallelization of computer codes plays a very important role, because it enables the code to run on multiple processors, resulting in considerable time-saving if the algorithm scales efficiently as the number of processors is increased progressively [32]. In order to take advantage of these clusters, it is necessary to modify the initial code, following a parallel-computation standard. The Message Passing Interface (MPI) paradigm [7] is at the present time widely used for the parallelization of codes based on the use of computer clusters.

The design of the parallel CBFM-MLFMA follows the so called data-parallel approach [33]. In this approach the data is partitioned among the processes, and each process executes approximately the same set of commands on its data. This approach usually leads to more scalable programs.

In the design of the parallel approach, all the groups are distributed between the processors [34]. Each group is assigned to a processor, which manages the information about all the coupling terms of the CBFs located in that group. In the delivering process, it is essential to apply load-balancing for the near-field. Each processor computes the near-field terms that correspond to the associated CBFs, and it obtains the rigorous coupling terms with the rest of CBFs by sharing information with other processors. Each processor calculates the aggregation and disaggregation terms of its assignated CBFs, and it exchanges this information at the corresponding level with those processors which require it.

In order to improve the efficiency of a parallelized program, the communication between processors and duplicated computations must be minimized. In a simple parallelization technique [32], we can obtain the highest level at which the MLFMA cubes are coupled. Next, we distribute and assign equally the cubes of that level to the processors, and, for the lower levels, if a cube in the higher-level belongs to a processor, then all its sub-cubes are also assigned to the same processor. By following this procedure, the aggregation and disaggregation steps from the bottom of the hierarchical tree up to the higher-coupling level can be performed without any communication.

This scheme avoids the communication between processors in the aggregation and disaggregation process, but it can lead to an inefficient speed-up in some cases. When the geometry of the scatter is irregular, by applying the higher-coupling level distribution a processor

can be in charge of cubes that have a low number of non-empty low-level cubes, so the processor can wait for long periods of time.

To overcome this disadvantage, a new strategy in the distribution of the cubes has been developed. We fixed the level of the distribution of the cubes to be different to the highest-coupling level. To avoid communication between processors in the aggregation and disaggregation processes for the cubes at a level above the distribution level, it is allowed that these cubes can be duplicated in different processors. For this cubes, each processor computes the aggregation of its sub-cubes, and adds its partial contribution in the translation process, so the contributions from different processors are combined automatically for the duplicated cubes. Applying this new strategy, the speed-up is improved for geometries with irregular shapes [35].

In Fig. 16 the speed-up for the COBRA cavity with a flap is shown. All the simulations have been performed using dual-core Opteron processors at 2.4 GHz with a total shared RAM of 64 GBytes. Table 2 shows the CPU-times for both polarizations using the presented approach, and a comparison between CBFM-MLFMA and MoM-MLFMA using the same parallelization scheme. The conventional CBFM CPU-time was 65966 seconds for each polarization with a single processor.

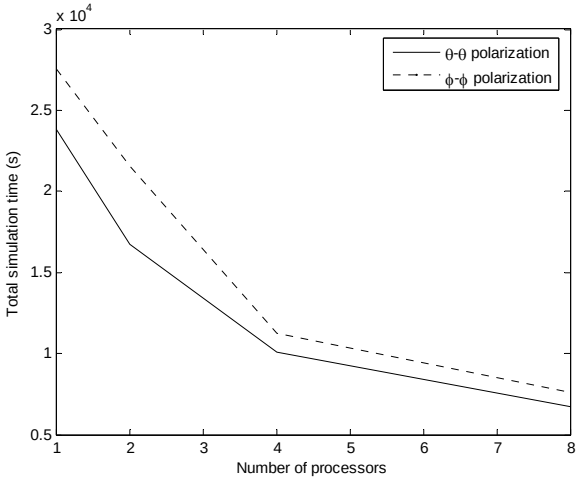

Fig. 16. Evolution of the CPU simulation time as a function of the number of processors.

Table 2. CPU-times for the simulations

Method	Polarization	N. of processors	Total CPU time	Preprocess time	Solver time
CBFM	Theta	1	23821 s	10567 s	13254 s
CBFM	Theta	2	16698 s	5276 s	11422 s
CBFM	Theta	4	10056 s	4146 s	5910 s
CBFM	Theta	8	6736 s	2401 s	4335 s
CBFM	Phi	1	27544 s	10650 s	16894 s
CBFM	Phi	2	21584 s	5353 s	16231 s
CBFM	Phi	4	11216 s	4195 s	7021 s
CBFM	Phi	8	7621 s	2417 s	5204 s
MoM	Theta	1	304443 s	743 s	303700 s
MoM	Theta	8	79095 s	177 s	78918 s
MoM	Phi	1	456756 s	743 s	456013 s
MoM	Phi	8	137154 s	177 s	136976 s

VI CONCLUSIONS

We have presented an overview of a very efficient, recently developed technique (CBFM), based on the definition of macro-basis functions which can be generated using different approaches. Also, we have presented an implementation of the CBFM combined with the MLFMA. The conventional MoM memory requirements are highly reduced due to the reduction of the number of unknowns via the CBFM and to the reduction in the size of the reduced matrix via MLFMA. Also the CPU-time is smaller due to the reduction of the size of the linear problem to be solved and to the efficiently computed matrix-vector products in the iterative solution process.

ACKNOWLEDGEMENT

This work has been supported in part by the University of Alcala and the Madrid Community Project CCG07-UAH/TIC-2058 and S-0505/TIC/0255. and by the Spanish Department of Education and Science Projects Ref. TEC2006-03140, TEC 2007-66164 and CONSOLIDER-INGENIO Nº CSD-2008-0068

REFERENCES

[1] G. T. Ruck, D. E. Barrick, W. D. Stuart, and C. K. Krichbaum, *Radar Cross Section Handbook*, Vol. 1, Plenum Press, 1970.

[2] D. A. McNamara, C. W. I. Pistorius and J. A. G. Maherbe, *Introduction to the Uniform Geometric Theory of Diffraction*, Norwood, MA: Artech House, 1990.

[3] U. Jakobus and F.M. Landstorfer: "Improved PO-MM hybrid formulation for scattering from three-dimensional perfectly conducting bodies of arbitrary shape", *IEEE Trans. Antennas Propagat.*, vol. 43, pp. 162-169, Feb. 1995.

[4] G. A. Thiele and G. A. Newhouse, "A Hybrid Technique for Combining Moment Methods with the Geometrical Theory of Diffraction", *IEEE Trans. Antennas Propagat.*, vol. 23, pp. 551-558, July 1975.

[5] W. D. Burnside, C. L. Yu, and R.J. Marhefka: "A technique to combine the geometrical theory of diffraction and the moment method", *IEEE Trans. Antennas Propagat.*, AP-23, pp. 551-558, July 1975.

[6] E. P. Ekelman and G. A. Thiele: "A hybrid technique for combining the moment method treatment of wire antennas with the GTD for curved surfaces", *IEEE Trans. Antennas Propagat.*, AP-28, pp. 831-839, November 1980.

[7] W. Gropp, E. Lusk, and A. Skjellum, *Using MPI*, MIT Press, October 1994.

[8] R. F. Harrington, *Field Computation by Moment Methods*, New York, McMillan, 1968.

[9] N. Engheta, W. D. Murphy, V. Rokhlin, and M. S. Vassiliou, "The Fast Multipole Method (FMM) for Electromagnetic Scattering Problems", *IEEE Trans. Antennas Propagat.*, vol. 40, no. 6, pp. 634-641, June 1992.

[10] W. C. Chew, J. Jin, E. Michielssen, and J. Song, *Fast and Efficient Algorithms in Computational Electromagnetics*, Artech House Inc., 2001.

[11] A. Boag and R. Mittra, "Complex multipole beam approach to electromagnetic scattering problems," *IEEE Trans. Antennas Propagat.*, vol. 42, pp. 366-372, Mar. 1994.

[12] F. X. Canning, "The Impedance Matrix Localization (IML) Method for Moment-Method Calculations", *IEEE Anntenas Propagat. Mag.*, vol. 32, no. 5, pp. 18-30, Oct 1990.

[13] E. Bleszynski, M. Bleszynski, and T. Jaroszewicz, "AIM: Adaptative Integral Method for Solving Large Scale Electromagnetic Scattering and Radiation Problems", *Radio sci.*, vol. 31, no.5, pp. 1225-1251, 1996.

[14] Gene H. Golub and Charles van Loan, *Matrix Computations*, Johns Hopkins University Press, 1989.

[15] R.J. Burkholder and J.F. Lee, "Fast Dual-MGS Block-Factorization Algorithm for Dense MoM Matrices", *IEEE Trans. Antennas Propagat.*, Vol-52, NO. 7, pp. 1693-1699, July 2004.

[16] M. Bebendorf, "Approximation of boundary element matrices", *Numer. Math.*, vol. 86, no. 4, pp. 565–589, 2000.

[17] K. Zhao, M. Vouvakis, and J. F. Lee, "The adaptive cross approximation algorithm for accelerated method of moment computations of EMC problems", *IEEE Trans. Electro. Comp.*, vol. 47, no. 4, pp. 763–773, Nov. 2005.

[18] E. Michielssen and A. Boag, "A multilevel matrix decomposition algorithm for analyzing scattering from large structures", *IEEE Trans. Electro. Comp.*, vol. 44, no. 8, pp. 1086–1093, Aug. 1996.

[19] L. Matekovits, V. A. Laza, and G. Vecchi, "Analysis of Large Complex Structures With the Synthetic-Functions Approach", *IEEE Trans. Antennas Propagat.*, vol. 55, no. 9, pp. 2509-2521, September 2007.

[20] V. V. S. Prakash and R. Mittra, "Characteristic Basis Function Method: A New Technique for Efficient Solution of Method of Moments Matrix Equation", *Micro. Opt. Tech. Lett.*, vol. 36, no. 2, pp. 95-100, Jan. 2003.

[21] S. M. Rao, D. R. Wilton, and A. W. Glisson, "Electromagnetic scattering by surfaces of arbitrary shape", *IEEE Trans. Antennas Propagat.*, vol. 30, pp. 409-412, May 1982.

[22] A. W. Glisson and D. R. Wilton, "Simple and Efficient Numerical Methods for Problems of Electromagnetic Radiation and

Scattering from Surfaces", *IEEE Trans. Antennas Propagat.*, vol. 28, no. 5, pp. 593-603, Sept. 1980.

[23] E. García , C. Delgado, I. González , and F. Cátedra, "An iterative solution for electrically large problems combining the Characteristic Basis Function Method and the Multilevel Fast Multipole Algorithm", *IEEE Trans. Antennas Propagat.*, accepted for publication.

[24] G. Farin, *Curves and Surfaces for Computer Aided Geometric Design: A Practical Guide*, Boston, Academic Press, 1998.

[25] E. Lucente , A. Monorchio, and R. Mittra, "An Iteration-Free MoM Approach Based on Excitation Independent Characteristic Basis Functions for Solving Large Multiscale Electromagnetic Scattering Problems", *IEEE Trans. Antennas Propagat.*, vol. 56, no. 4, pp. 999-1007, April 2008.

[26] C. Delgado, R. Mittra, and F Cátedra, "Accurate Representation of the Edge Behavior of Current when Using PO-Derived Characteristic Basis Functions", *IEEE Antennas and Wireless Propagat. Lett.*, vol. 7, pp. 43-45, March 2008.

[27] G. Tiberi, M. Degiorgi, A. Monorchio, G. Manara, and R. Mittra, "A Class of Physical Optics-SVD Derived Basis Functions for Solving Electromagnetic Scattering Problems", *Antennas and Propagation Society Int. Symposium*, Washington D.C, USA, July 2005.

[28] C. Delgado, F. Cátedra, and R. Mittra: "Application of the Characteristic Basis Function Method Utilizing a Class of Basis and Testing Functions Defined on NURBS Patches", *IEEE Trans. Antennas Propagat.*, vol. 56, no. 3, pp. 784-791, March 2008.

[29] L. Valle, F. Rivas, and M. F. Cátedra, "Combining the Moment Method with Geometrical Modelling by NURBS Surfaces and Bézier Patches", *IEEE Trans. Antennas Propagat.*, vol. 42, no. 3, pp 373-381, March 1994.

[30] M. F. Cátedra, F. Rivas, and L. Valle: "A Moment Method Approach Using Frequency Independent Parametric Meshes", *IEEE Trans. Antennas Propagat.*, vol. 45, no. 10, pp. 1567-1568, October 1997.

[31] J. Liu and J. Jin, "Scattering Analysis of a Large Body with Deep Cavities", *IEEE Trans. Antennas Propagat*, Vol. AP-51, Issue 5, pp 1157-1167, June 2003.

[32] A. K. Dominek, H. Shamanski, R. Wood, and R. Barger, "A Useful Test Body", *in Proceedings Antenna Measurement Techniques Association*, September 24, 1986.

[33] Özgür Ergül and Levent Gürel, "Efficient Parallelization of Multilevel Fast Multipole Algorithm". *Proceedings of the European Conference on Antennas and Propagation: EuCAP 2006.* Nice, France, November 2006.

[34] P. S. Pacheco, *Parallel Programing with MPI*, Morgan Kaufmann Publishers Inc., 1997.

[35] W. C. Chew, J. Jin, E. Michielssen, and J. Song, *Fast and Efficient Algorithms in Computational Electromagnetics*, Artech House Inc., 2001.

[36] E. García, C. Delgado, I. González, and F. Cátedra "A Parallel CBFM-MLFMA Implementation for the Analysis of Complex Problems" *ACES 2008 Meeting*, April 2008.

Carlos Delgado was born in Guadalajara, Spain, in 1979. He received the MS degree in Telecommunications Engineering from the University of Alcalá, Spain, in 2002, and the Ph. D. in Telecommunications Engineering in 2006. He is currently an Associate Professor in the Computer Science Department, Universidad de Alcalá, Spain. He was a visiting scholar during fall 2005 and a visiting postdoctoral fellow during spring and summer 2007 at the Electromagnetic Communication Laboratory of the Pennsylvania State University. His research interests include numerical methods applied to scattering and radiation problems, hybridization of high frequency and numerically rigorous methods and fast computational techniques applied to electromagnetics.

Eliseo García was born in Madrid, Spain, in 1977. He received the B.S., M.S. and Ph.D. degrees in telecommunication engineering from the University of Alcalá, Spain, in 1999, 2001 and 2005, respectively.Since 2005, he worked at the University of Alcalá, first as Assistant Professor and since 2006 as Associated Professor in the Automatic Department. His research interests include numerical methods applied to scattering and radiation problems, parallel computing and fast computational techniques applied to electromagnetics.

Manuel F. Catedra received his M.S. and Ph. D. degrees in Telecommunications Engineering from the Polytechnic University of Madrid (UPM) in 1977 and 1982, respectively. From 1976 to 1989 he was with the Radiocommunication and Signal Processing Department of the UPM. He has been Professor at the University of Cantabria from 1989 to 1998. He is currently Professor at the University of Alcalá, in Madrid, Spain. He has worked on about 80 research projects solving problems of Electromagnetic Compatibility in Radio and Telecommunication Equipment, Antennas, Microwave Components and Radar Cross Section and Mobile Communications. He has developed and applied CAD tools for radio-equipment systems such as Navy ships, aircraft, helicopters, satellites, the main contractors being Spanish or European Institutions such as EADS, ALCATEL, CNES, ALENIA, ESA, DASA, SAAB, INTA, BAZAN, INDRA, and the Spanish Defence Department. He has directed 16 Ph. D. dissertations, has published about 55 papers (IEEE, Electronic Letters, etc), two books, about 10 chapters in different books, has given short courses and has given more than a hundred and thirty presentations in International Symposia.

Raj Mittra is Professor in the Electrical Engineering department of the Pennsylvania State University. He is also the Director of the Electromagnetic Communication Laboratory, which is affiliated with the Communication and Space Sciences Laboratory of the EE Department. Prior to joining Penn State he was a Professor in Electrical and Computer Engineering at the University of Illinois in Urbana Champaign. He is a Life Fellow of the IEEE, a Past-President of AP-S, and he has served as the Editor of the Transactions of the Antennas and Propagation Society. He won the Guggenheim Fellowship Award in 1965, the IEEE Centennial Medal in 1984, the IEEE Millennium medal in 2000, the IEEE/AP-S Distinguished Achievement Award in 2002, the AP-S Chen-To Tai Distinguished Educator Award in 2004 and the IEEE Electromagnetics Award in 2006. He has been a Visiting Professor at Oxford University, Oxford, England and at the Technical University of Denmark, Lyngby, Denmark. He has also served as the North American editor of the journal AEU. His professional interests include the areas of Communication Antenna Design, RF circuits, computational electromagnetics, electromagnetic modeling and simulation of electronic packages, EMC analysis, radar scattering, frequency selective surfaces, microwave and millimeter wave integrated circuits, and satellite antennas.He has published over 900 journal and symposium papers and more than 40 books or book chapters on various topics related to electromagnetics, antennas, microwaves and electronic packaging. He also has three patents on communication antennas to his credit. He has supervised 90 Ph.D. theses, 90 M.S. theses, and has mentored more than 50 postdocs and Visiting scholars. He has directed, as well as lectured in, numerous short courses on Computational Electromagnetics, Electronic Packaging, Wireless antennas and Metamaterials, both nationally and internationally.